The potential and advances of cryo-ET: unravelling structural heterogeneity *in situ*

Jolijn Govers, student number 5642248, master student Molecular and Cellular Life Sciences, Utrecht University

Supervised by Dr. Martin Beck of the MPI for biophysics, Frankfurt

Second supervisor: Prof. Dr. Friedrich Förster of Utrecht University

Layman's Summary

Organisms are composed of cells, which are mostly too small to be observed by the naked eye and are studied with a microscope. In turn, cells themselves contain a hidden world, with a wide variety of different molecules. These molecules all have specific functions to make sure that cells can communicate with each other, divide, migrate and undertake a wide variety of other activities needed for them, and in turn an organism, to function. In addition, these molecules can also cause or prevent diseases. Therefore, to understand live, it is crucial to understand how the molecules inside those cells function. One way of doing this is solving the structure of these molecules and molecule complexes.

Since they are so incredibly small, molecules can only be imaged using special, high-resolution techniques such as electron microscopy. To obtain a high-resolution model of a molecule or a complex of molecules, these molecules can be extracted from their environment. The resulting homogeneous samples are then be subjected to an electron beam, resulting in an image of many identical molecules. Since especially the high-resolution features are difficult to distinguish during image acquisition, the different 2D images of the molecule are taken together to get a 3D reconstruction of the molecule.

However, there are usually a lot of different molecules working together inside a cell. Therefore, molecules in their native environment might be interacting with or influenced by other molecules and have a different conformation than when the molecule is purified. Therefore, imaging molecules within their natural environment is of great importance.

Until recently, there were several factors that hampered this. Electron microscopy (EM) depends on electrons passing through a specimen. However, cells are thicker than a single layer of molecules extracted from them, so less electrons make it through, resulting in an image with a lower signal compared to the noise. To overcome these problems, samples of cells can nowadays be thinned using a focused ion beam. The thinned biological samples are rotated during image acquisition, to obtain a 3-dimesional view of the specimen. From this, the molecules of interest are picked, aligned, and averaged, hereby increasing the signal of the molecules in comparison to the noise. This method to obtain structures directly from their cellular (*in situ*) environment is called *in situ* cryo-electron tomography (CET).

This method has been used to solve one of the most fundamental processes going on in cells, which is the transcription of DNA into an in this case molecule called RNA. Some RNAs are subsequently translated into proteins, which account for most of the processes in the cell. This process of transcription and translation is tightly coupled, and using *in situ* CET, researchers were able to identify which molecules are involved in these processes, how they interact and the mechanism by which these processes are coupled.

Abstract

The resolution revolution has made cryo-electron microscopy an increasingly popular technique to study the structural biology of purified macromolecules and complexes. Extraction of these complexes can have a profound effect on their conformation since biomolecules are usually subject to modifications of and interactions with their native environment. Cryo-electron tomography (cryo-ET) presents a powerful approach to examine macromolecules *in situ*, enabling the high-resolution visualisation of the molecular organisation and localisation within the cell. In this review, I'll discuss the cryo-EM and cryo-ET workflow, and I will elaborate on how these recent technical advancements contributed to resolving the mechanism of translation-transcription coupling in prokaryotes.

Introduction

Organisms depend on an intricate network of proteins, nucleic acids, and their interactions for cell growth and proliferation. Structural biology aims to understand the function and mechanism of these molecules at the molecular level by deriving their 3D structure.

Conventionally, proteins, nucleic acids, and complexes are purified from lysed cells and studied by one of the structural biology methods available, such as X-ray crystallography, nuclear resonance microscopy (NMR) or cryo-electron microscopy(EM)[1]. The most prominent way to do this in the past has been X-ray crystallography, which involves purification of proteins and nucleic acids or complexes and subsequent crystallisation. This technique provides a high resolution but is limited by the crystallisation potential of the target molecules[2]. NMR facilitates studying interactions, dynamics and alternate conformations of the investigated proteins and nucleic acids, but structure determination is limited to molecules and complexes smaller than 50 kDa[3]. Cryo-EM overcomes these crystallisation and size-limit restraints and has gained in popularity due to the recent resolution revolution, reaching near-atomic resolutions[4,5,6]. Structures are most commonly reconstructed using single particle analysis (SPA), which combines a multitude of 2D molecule images to obtain a high-resolution 3D structure.

Although these techniques have contributed considerably to our understanding of molecular biology, the resulting information is limited due to the extraction of the molecules out of their native environments[7]. Biomolecules only seldomly function on their own and they are frequently subjected to modifications and influences of their environment, which often makes it hard to determine the accuracy and implications of the structures found[8]. For example, it is initially unclear whether the macromolecule is part of a complex that is filtered out and how accurate the conformations identified are. Biochemical reconstructions are required to clear these types of uncertainties up. Cryo-electron tomography (CET) overcomes these problems by providing *in situ* structural information, which in addition also provides spatial information on the localization of the macromolecule and even different macromolecule conformations within a specimen[9,10]. Due to the low signal-to-noise ratio (SNR) of *in situ* samples, they must be tilted over a range of angles. The 3D macromolecules of interest can then be aligned and averaged to increase the SNR and resolve a high-resolution structure.

Recent advancements in sample preparation and data processing strategies have brought a set of improvements such as a higher achievable resolution and a wider range of samples that

can be studied[11]. As a result, an increasing number of molecular systems has been assessed structurally *in situ*, leading to novel insights into macromolecular assemblies that had remained ambiguous to traditional structural biology, amongst which the coupling of the translation-transcription machinery of prokaryotic cells[8].

This review provides an overview of the general workflow of cryo-EM for single particle analysis (SPA) and *in situ* tomography and highlights recent advancements. In addition, I will discuss how these techniques have contributed to the research on the prokaryotic transcription-translation machinery.

Cryo-Electron Microscopy and its Recent Developments

To obtain a 3D structure using cryo-EM, samples are prepared, subjected to electron microscopy and the resulting data is processed[12,13]. Based on the research aims, objects and cryo-EM method, each sample requires specific preparation. The most widely used methods are single particle (SP) cryo-EM and CET. Single particle cryo-EM provides high resolution data of structures outside of their native environment, while CET is performed *in situ*, allowing macromolecules to be reconstructed within their crowded native environment. Although many similarities exist between the SP cryo-EM and CET workflows, there are some profound differences. In this section, I'll delve into the different steps in the workflow and highlight recent advancements.

Sample grid preparation

Sample grid preparation consists of three main steps: sample preparation, vitrification, and thinning (Fig. 1). The specifics of these steps are dependent on the type of sample and cryo-EM method.

In single particle cryo-EM, an ideal sample requires an adequate concentration of intact macromolecules on the grid. While the preparation of a single grid is straightforward, the numerous biochemical assays required to be able to extract a macromolecule in a native structural conformation may be tedious[7]. As a result, sample preparation is a major bottleneck in the cryo-EM workflow. After sample preparation, samples are vitrified for sample stabilization, protection from the high vacuum of the EM, and limiting radiation induced damage[14]. This should ideally result in a monolayer of macromolecules on the grid.

In situ CET samples can be vitrified immediately, avoiding the biochemical assays needed for SPA preparations. *In situ* specimen with a thickness of up to ~5 µm can be plunge-frozen; specimen that supersede this limit can be frozen using high-pressure freezing[16]. Since transmission electron microscopy (TEM) requires electrons to pass through the sample, sample thickness is limited to approximately 300 nm, rendering the majority of cell types and tissues too large for image acquisition. Therefore, cellular specimen often require an additional step of sample thinning. Several techniques have been developed for sample thinning, amongst which thin sectioning of vitreous samples[18] and cryo-focused ion beam (FIB) milling[19]. The type of technique that is most suited depends on sample thickness and on the research aims.

Thin sectioning with CEMOVIS leaves artefacts that compromise the resolution, resulting in FIB milling being the method of choice to obtain high-resolution structures[20]. FIB milling enables lamellae to be milled to thicknesses well-suited for CET, between 60 and 350 nm, by subjecting the areas above and beneath the area of interest to a focused beam of Gallium ions, allowing precise milling in a stable vacuum and cryo-temperature environment[19]. By monitoring the sample with a scanning electron microscope (SEM) and ion beam imaging, the thinning process can be followed in real-time[21]. Although this technique has provided some remarkable results, its output is limited. This is caused by the technique's high-cost, limited efficiency, and requirement for the full-time presence of a skilled user. For a high-resolution dataset, several high-quality lamellae are needed. To increase the efficiency, an automated workflow has been introduced recently, hereby also making the technique more accessible

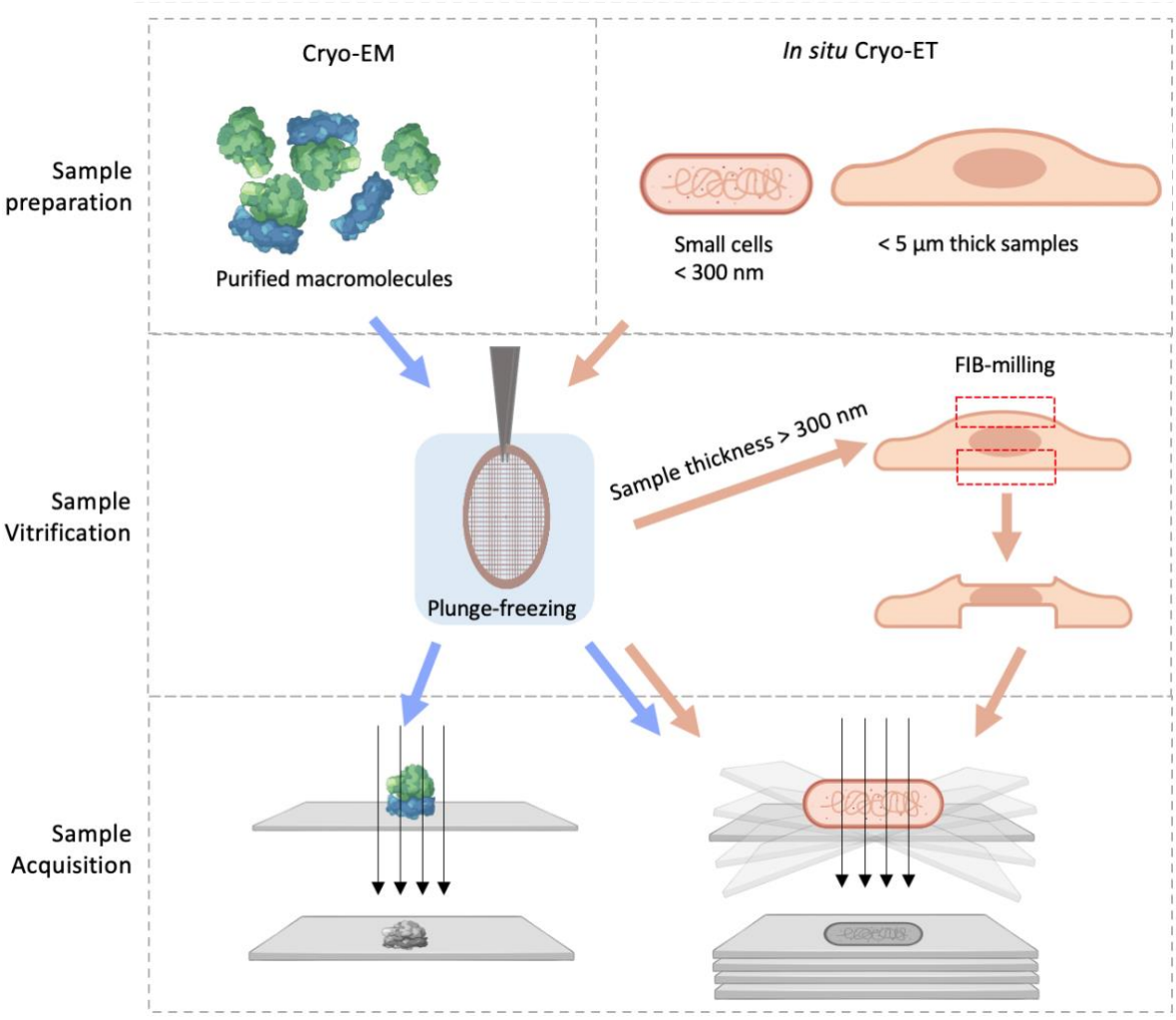

Figure 1: cryo-EM and ET workflow from sample preparation and image acquisition for high-resolution structure determination. Samples for single particle cryo-EM are prepared through purification, added onto a grid, and vitrified by plunge freezing. Data acquisition results in a 2D image. SPA datasets can optionally also be acquired with tomography. For *in situ* cryo-ET, intact cells of up to 5µm thickness are added onto a grid and plunge frozen. Samples with a thickness of < 300 nm directly acquired; larger samples up to 5 µm are thinned by focused-ion-beam (FIB)-milling. Next, images are acquired using an electron beam over several tilting-angles, resulting in a series of tilt images. Blue arrows indicate the workflow of cryo-EM for SPA. Orange arrows indicate the workflow of *in situ* CET.

to unexperienced users[22,23]. These challenges can be avoided when smaller specimen such as bacteria are studied with *in situ* cryo-ET, since many of these cells are small enough to not require any thinning, hereby drastically reducing sample preparation times.

Another potential difficulty in *in situ* cryo-ET is identifying the target molecule in the intricate, highly packed complexity of a cell. Whereas samples for SPA are enriched with the macromolecules of interest, *in situ* samples are eminently heterogenous and crowded, which makes it hard to identify molecules that are less abundant or do not belong to the largest complexes present in the cell. Therefore, several methods have been developed to facilitate the localisation of the target molecule or even rare events within the cell. Correlative light and electron microscopy (cryo CLEM) can be used to identify an area of interest and hereby guide potential FIB-milling and data acquisition[24]. To overcome the gap in resolution between fluorescence (250-400 nm resolution) and electron microscopy (images of 2-10 nm), several groups have been working on the application of super-resolution imaging, resulting in a localization precision of 10 nm to 20 nm[25,26]. By providing more insight into the localisation of the target macromolecules, this method has the potential to contribute to the overall understanding of the molecule and its functions. Due to the complexity of these techniques, large and abundant macromolecules like ribosomes have been subject of research most predominantly.

Data acquisition on the TEM

Detectors

As a next step of the workflow, specimen-holding grids are loaded into the cryo-electron microscope, where each is subjected to a high-energy electron beam. The beam causes beam-induced motion (BIM) of the sample, leading to a change in particle orientations and positions and affecting the obtainable resolution[27]. With the state-of-the-art detectors having a frame rate of up to 15,000 frames per second (K3, Gatan), an array of frames can be taken in such a rapid succession from an area of interest that it provides a great resource for beam-induced motion (BIM) correction[27,28]. In addition, these direct electron detectors lead to an improved detective quantum efficiency (DQE), hereby reducing the electron dose required to acquire an image of a similar quality[29]. These improvements have had an considerable impact on resolution revolution in cryo-EM[30].

Image formation

Image formation of transmission electron microscopy (TEM) is dependent on the elastic scattering of electrons by the sample and can be affected by inelastic scattering, multiple scattering events, and beam and sample induced convolution.

Inelastically scattered electrons reduce the obtainable resolution by directly interfering with image formation[31] and causing sample damage, hereby leading to structure deformation upon accumulation[14]. To limit the number of such inelastic scattering events, images are acquired with high-energy electrons in combination with a low electron dose[32]. For cryo-ET acquisition of images with a low electron dose poses an extra problem since a TS usually consists of around 20 to 40 images to achieve a good resolution[33]. To limit beam damage, the dose is distributed over the tilts, resulting in a lower contrast of weak phase objects[8].

Image formation distortion by multiple scattering events is correlated by sample thickness, leading to a reduced SNR for thicker samples[34]. Considering that sample thickness increases upon increased tilt angle, higher tilting angles contain a decreased SNR. The effects of inelastic scattering and tilting angle on the resulting image pose a dilemma of which tilt-scheme is optimal for data acquisition. The dose-symmetric scheme acquires incrementally, toggling between plus and minus angles[35]. High-resolution containing low-tilt angles are acquired first before the onset of beam induced damage, hereby optimizing the beam-induced damage at certain tilts. Although this contributes to a higher resolution, the time and resources required are high. Since high resolution datasets also require hundreds to thousands of TS, a continuous tilting scheme has been developed, that utilizes continuous tilt acquisition[36]. By skipping steps that are required in a dose-symmetric scheme, sub-nanometre structures can be achieved within an hour of acquisition time, facilitating a higher data throughput.

The amplitude of electrons scattered by biological molecules is neglectable in comparison to the primary beam, this resulting in a low contrast. In addition, image formation of biological samples is convoluted by the contrast transfer function (CTF)[37] as a result of their weak electron scattering capacity and the spatial and temporal incoherence of the electron beam. The CTF is an envelope-shaped sinewave that describes the correlation between spatial frequency and intensity[37]. By acquiring a frame in defocus, the limit of detectable high spatial frequencies is increased. However, due to the sinewave-nature of the CTF, spatial frequencies where the CTF passes zero are lost and can't be recovered. In an attempt overcome this hurdle, several phase plates have been developed that enhance the contrast through induction of an additional phase shift of the scattered electrons in comparison to the primary electron beam[38]. However, these phase plates limit the resolution by imposing time- and space-dependent phase shifts, which is to be overcome with laser phase plates that are currently under development[39].

Data processing

General Pipeline

To obtain structural information of the molecule of interest, the collected images require several processing steps. In SPA, the basic workflow consists of BIM and CTF correction of the collected images, particle picking and extraction[12] (**Fig. 3**). Next, high-resolution structural details can be resolved from the low SNR datasets by averaging multiple copies of repetitive features. Lastly, reconstructed particles may be refined and 3D classified if required.

Single Particle Analysis

As a first step in the SPA processing pipeline, the frames that reconstitute an image are aligned to correct for sample motion and increase the sharpness of the image[12]. Individual frames are correlated to each other using gold-fiducial markers or fiducial-less methods such as patch-tracking[45]. Gold-fiducial markers provide a strong SNR and therefore provide better alignment in comparison to fiducial-less methods that rely on low SNR data for alignment. Aligned images are used as input for CTF determination. The CTF is usually estimated by fitting a theoretical CTF curve to the power spectrum of an image to estimate the defocus, phase-flipping the negative CTF values and dividing the intensity by the CTF values[47].

After these pre-processing steps, the quality of the reconstructed 2D SPA is sufficient for particle picking, extraction and averaging the extracted particles iteratively to obtain a high-resolution reconstruction of the particle. Particles can be picked from the reconstructed volumes in several ways, including picking by hand or automated picking. SPA particles can be automatically picked using template or template-free methods, for which several neuronal network-based methods have recently been developed[51,52,42]. The picked particles are extracted in 2D as input for SPA, where the different copies of the randomly oriented macromolecule are aligned and averaged. Upon combination with a great number of additional images, the 3D reconstructed macromolecule can reach a high-resolution.

STA

CET processing consists of similar steps but requires an additional step of tomogram alignment and reconstruction prior to particle picking (**Fig. 3**)[40]. Images of a tilt-series are also shifted amongst each other and therefore require an additional alignment step. Gold-fiducial markers can often not used in CET samples as a result to their inability to diffuse through the cell, resulting in datasets to be aligned using patch-tracking.

After alignment, the tilt-series can be reconstructed by the weighted back-projection (WBP), that reconstructs the 3D Fourier transform (FT) from 2D FTs[46]. A properly aligned and reconstructed stack of projections is a key step for further processing, especially particle picking.

CET processing must overcome additional complications to reliably approximate the CTF. For one, the lower SNR makes it more difficult to accurately estimate the defocus. In addition, as a consequence of tilting, variation of defocus values arises along the sample. Lastly, tomography is usually performed on thicker samples, in which scattering objects are located at different Z-heights within the sample and therefore have considerably different defoci. Recently, novel algorithms have been developed for 3D-CTF correction, contributing to a higher resolving power of STA[48,49,50].

Particle picking in *in situ* CET tomograms is complicated by the high biochemical complexity and a low SNR of the dataset. Therefore, this technique usually requires a template, for which a reference obtained from the dataset itself is preferable to avoid a bias. A variety of software has been developed to aid the process[53,44,54], amongst which deep learning-based methods[55,56]. Due to the particle picking difficulties of *in situ* datasets, the size of molecules that can be picked and therefore resolved is limited to 500 kDa, compared to ~100 kDa in SPA[13]. The picked particles are extracted in 3D as input for STA.

STA is based on similar principles as SPA, averaging particles in order to resolve structures to increase the SNR and reach a high resolution[57]. However, *in situ* tomographs require a 3D reconstruction method to avoid disruption of the image organelles located in different planes of the volume. The 3D nature of the tomogram eases subtomogram alignment and averaging.

Whereas SPA is routinely used, subtomogram averaging (STA) is less commonly used because of the added complexity of the processing, and the lack of a streamlined, user-friendly pipeline. Though previously users commonly had to work with a patchwork of software[41,11],

several programs are under development to integrate all processing steps and increase and ease the CET throughput[41,42,43,44].

Refinement, classification, and interpretation

In tomography additional refinement methods are required to obtain a higher resolution structure. As previously discussed, alignment of TS images is a key step to obtain good subtomogram averages. Since the initial, conventional alignment methods are still global, further refinement can make a great difference to obtain a higher resolution. Therefore, Tegunov and colleagues have recently developed a technique that performs a per-particle, 3D alignment based on motion models called M[28]. Using high detector frame rates to capture local sample movements, M corrects for translation, rotation, doming and image- and volume-space warping sample movements and deformations. M still needs a reasonable initial alignment quality, so an initial alignment with gold-fiducial markers allowed for a good

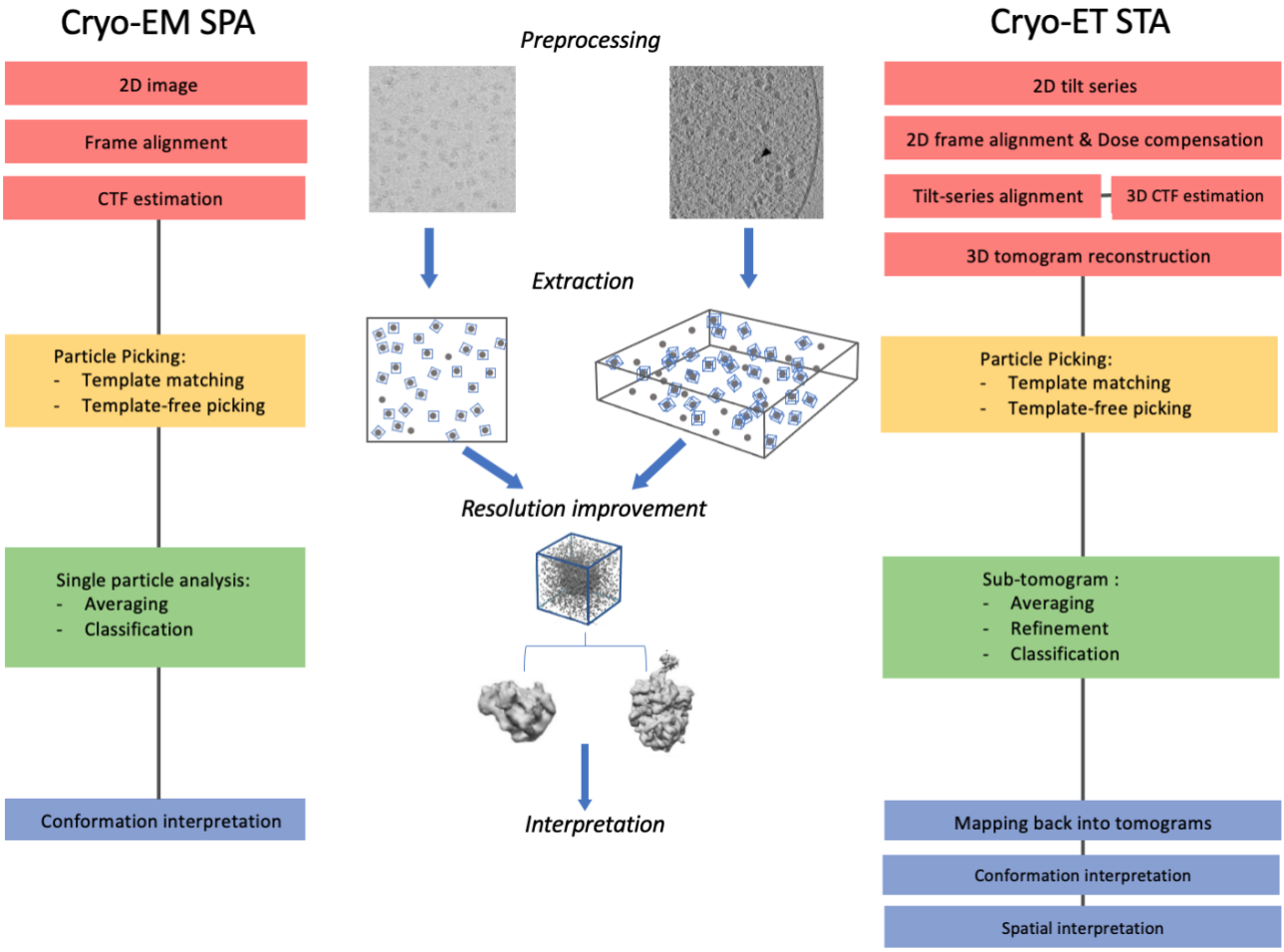

Figure 2: cryo-EM and ET processing pipeline. The workflow consists of four parts, image/tomogram reconstruction (red), particle picking (yellow), resolution improvement (green), and data interpretation (blue). Major differences between the cryo-EM and cryo-ET workflows consist of additional steps in tomogram reconstruction and the use of SPA versus STA. After particles are reconstructed, cryo-ET derived reconstructions can be placed back into the tomogram. Figure modified from Turk & Baumeister (2020). SPA EM map from Kohler et al. (2017). STA EM map and classification averages from O'Reilly et al. (2020).

quality of alignment refinement, which lead to the first high-resolution *in situ* study of the expressome[58].

The ongoing resolution improvements in cryo-EM allow researchers to resolve a higher variety of molecule conformations, improving further refinement using classification. By classifying macromolecules with a heterogeneous conformation, time-resolved cryo-EM is now attainable[59]. Until recently, such time-resolved *in situ* cryo-ET was out of reach due to resolution limitations. As a result of the latest improvements of reconstruction quality of M, such time-resolved *in situ* structural analysis is achievable, as research on the translation dynamics in bacterial cells recently showed[10]. In addition to the identification of a variety of transitional conformations, Xue and colleagues managed to project the specific conformations back into the cell, hereby further insight into the spatial relationships and functions of these conformations.

Integrative Methods

Data integration of additional methods is used to further boost the resolution, increase the understanding of structural dynamics, obtain spatial information and investigate molecule interactions a structural level[60,61]. For example, high-resolution X-ray structures are commonly fitted to the lower-resolution cryo-EM reconstructions to help correctly interpret the densities[8]. In *in situ* macromolecule reconstruction, higher-resolution SPA structures are also commonly used for structure interpretation. Further improvements can be made using computational models, and such as the recently artificial intelligence methods to predict protein structures and interactions[62].

Integration of mass-spectrometry with cryo-EM provides a tool to investigate the molecular sociology of the molecule of interest[63]. Quantative MS can provide insight into both the molecular components of a complex and their stoichiometry[64]. Cross-linking MS is often used in combination with *in-situ* CET to identify additional interaction partners and interaction sites. This information can be used to identify and model the identified molecules in unspecified densities of the subtomogram averages[65], which facilitated the identification of the composition of the translation-transcription complex in *M. pneumoniae*[66].

Macromolecules undergo rapid conformational changes, of which conventional cryo-EM and cryo-ET only manage to obtain some intermediate snapshots of the structures, overlooking essential transient conformations. By integrating cryo-EM techniques with techniques such as NMR, FRET and time-resolved MS, an improved understanding of the structural dynamics of macromolecular complexes such as the translation machinery could be attained[67,68].

Transcription-translation coupling in prokaryotes

In this next section I'll discuss the developments in the identification of expressome conformations and highlight how recent advancements in cryo-EM and cryo-ET have enabled these discoveries.

The transcription-translation machineries are among the most studied complexes, performing highly conserved processes. Whereas eukaryotes confine these processed to different compartments, they occur in close proximity in prokaryotes. Synchronized transcription and translation coordination is essential for cell viability[69]. The mechanism of

this coupling is still elusive. RNAP pauses regularly during translation, potentially leading to premature transcription termination. By pushing the RNAP forward, the trailing ribosome promotes transcription attenuation and aids the coordination of transcription and translation[70]. Several studies suggested that a reverse interaction of the ribosome with the RNAP also exists, it is unclear whether this interaction is direct or indirect[71]. Transcription is assisted by the transcription elongation complex (TEC) that regulates transcription. Proteins NusA and NusG are part of this complex and have been shown to function in transcription and translation coupling, influencing both transcription termination and antitermination.

Initial cryo-EM structures resolved by the purification of stalled RNAP-ribosome complexes showed a tightly packing RNAP-ribosome complex[72]. In this conformation, the RNAP mRNA exit tunnel is in such close proximity of the 30S ribosome mRNA entry tunnel, that it seamlessly shields the mRNA, which lead to the believe that the ribosome does interact with RNAP physically. However, additional studies showed that stalling of ribosomes does not affect translation elongation, which contradicts the direct physical ribosome-RNAP interaction[73].

Advances in cryo-EM and cryo-ET facilitated two recent studies that were able to resolve a range of expressome conformations that helped understanding of the mechanism of transcription-translation coupling (Fig. 3).

Recent progress in cryo-EM enabled SPA of samples with more heterogeneity, allowing for the identification of multiple conformational states and for the use of more heterogenic samples. This facilitated a 3.0 Å nominal resolution reconstruction of the *E. coli* expressome in alternate conformations obtained with single particle cryo-EM[74]. The resulting reconstruction showed an uncoupled expressome, with RNAP adopting a range of different rotations around the mRNA entrance channel of the ribosome. An alternative conformation shows physical coupling and tethering of the RNAP and ribosome by a NusG bridge. In addition, the research showed how a decreased mRNA length between the ribosomal P-site and the RNAP active site[74] resembled the previously reconstructed structure by Kohler et al., representing a collided expressome, in which NusG was no longer connected to the ribosome[72]. To obtain these conformations, the concentration of NusG was increased to ensure saturation of the NusG binding sites, which showcases the ease of which such samples can be manipulated.

At the same time, the improvements in *in-situ* cryo-ET lead to higher resolution reconstructions and broadened the possibilities of conformation classification[28]. This led to the publication of a series of structures of the *in-situ M. pneumoniae* expressome[66]. The identified classes display the structural dynamics of the transcription-translation conformation, comprising coupled, uncoupled and collided complexes. Classification additionally led to the identification of ribosome tRNA occupancy states of the *in-situ* ribosomes, allowing for distinction between actively elongating and paused complexes.

In addition to providing an *in-situ* expressome conformation, O'Reilly et al. used integrative *in-situ* cross-linking MS to obtain the molecular sociology of the expressome, hereby identifying a difference in interaction of the ribosome and RNAP with NusA and NusG in *M. pneumoniae* compared to *E. coli*[66]. Whereas previous research indicated RNAP and ribosome to be bridged by NusG in *E. coli*[75], the MS data suggested that in *M. pneumoniae* this bridge consists of NusA instead. Since several regions of NusA and NusG that are involved in physical interactions with RNAP and ribosomes differ substantially between the two species, this explains the difference observed binding modes and overall conformations[75]. However, an additional explanation for the observed differences could also be the presence of additional translation factors in the *in-situ* sample. For example, the elongation factor EF-G stabilises the post-translocation state that can be observed in the collided-expressome, while the ribosome in the *in vitro* expressome is trapped in an alternative translational state. Therefore, it would be interesting to also *in-situ* information in *E. coli*, to be able to address the differences in organism and in environmental surrounds of the resolved complex.

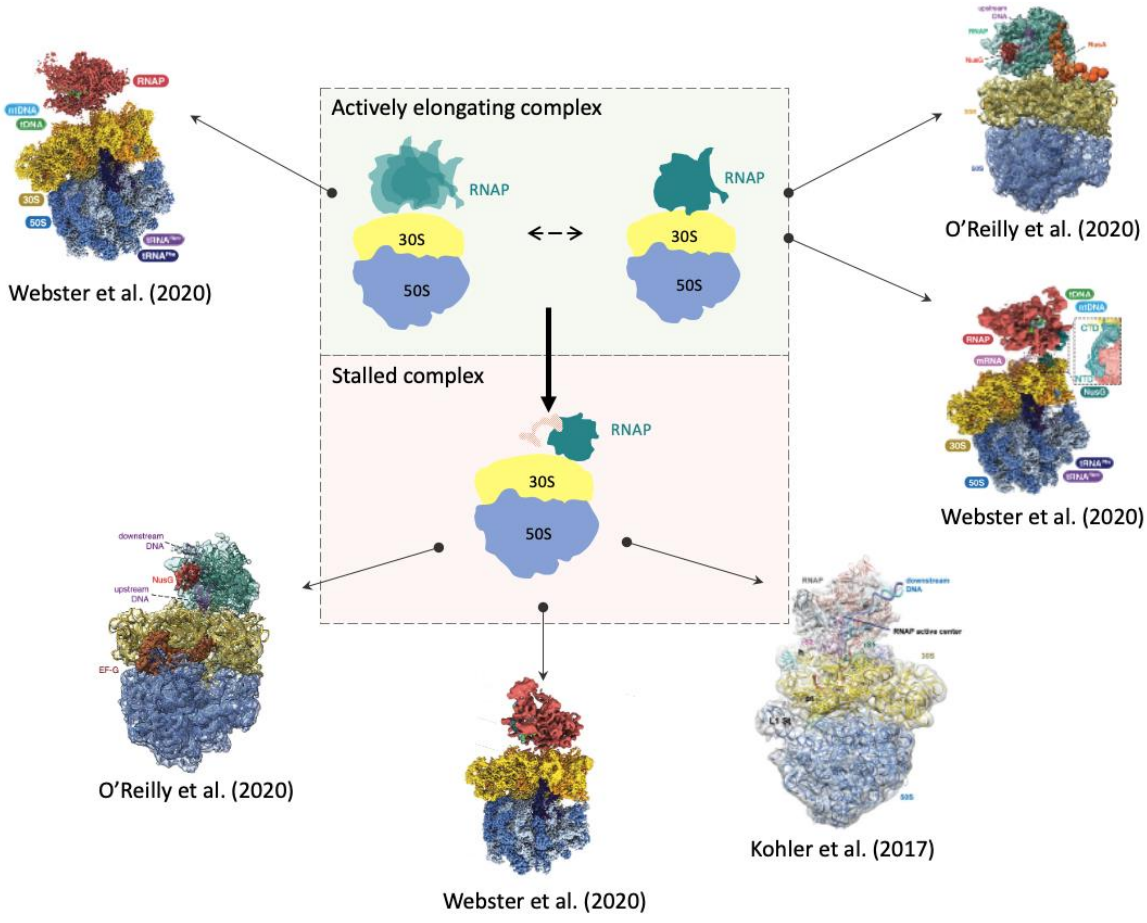

Figure 3: The relationship between expressome conformation and activity identified using cryo-EM and* in situ *CET. The green-boxed schematic representation of the expressome on top shows the conformations that are related to an actively elongating complex and the orange-boxed drawing on the bottom represents the collided, stalled complex. The arrows pointing from a representation point to structures found using cryo-EM from Kohler et al. (2017) and Webster et al. (2020), and CET O'Reilly et al (2020).

Concluding Remarks

Cryo-EM and *in-situ* cryo-ET continue to improve and evolve, resulting in higher resolutions, an even broader set of applications and an increasingly accessible and automated processing workflow. New processing strategies has improved the feasibility of classification in *in-situ* cryo-ET, allowing for time-resolved *in-situ* structure determination. However, several major obstacles still must be overcome to make the technique available to a larger public, of which sample preparation, limitations in sample size, target identification and data processing software usability are still considerable bottlenecks. Further automation of these obstacles will improve the usability of cryo-ET.

References

1. Bai, X. chen, McMullan, G. & Scheres, S. H. W. How cryo-EM is revolutionizing structural biology. *Trends Biochem. Sci.* **40**, 49–57 (2015).
2. Rossmann, M. G., Morais, M. C., Leiman, P. G. & Zhang, W. Combining X-ray crystallography and electron microscopy. *Structure* **13**, 355–362 (2005).
3. Alderson, T. R. & Kay, L. E. NMR spectroscopy captures the essential role of dynamics in regulating biomolecular function. *Cell* **184**, 577–595 (2021).
4. Saibil, H. R. Cryo-EM in molecular and cellular biology. *Mol. Cell* **82**, 274–284 (2022).
5. Nakane, T. *et al.* Single-particle cryo-EM at atomic resolution. *Nature* **587**, 152–156 (2020).
6. Yip, K. M., Fischer, N., Paknia, E., Chari, A. & Stark, H. Atomic-resolution protein structure determination by cryo-EM. *Nature* **587**, 157–161 (2020).
7. Weissenberger, G., Henderikx, R. J. M. & Peters, P. J. Understanding the invisible hands of sample preparation for cryo-EM. *Nat. Methods* **18**, 463–471 (2021).
8. Beck, M. & Baumeister, W. Cryo-Electron Tomography: Can it Reveal the Molecular Sociology of Cells in Atomic Detail? *Trends Cell Biol.* **26**, 825–837 (2016).
9. Pfeffer, S. & Mahamid, J. Unravelling molecular complexity in structural cell biology. *Curr. Opin. Struct. Biol.* **52**, 111–118 (2018).
10. Xue, L. *et al.* Visualizing translation dynamics at atomic detail inside a bacterial cell. *bioRxiv* 2021.12.18.473270 (2021).
11. Böhning, J. & Bharat, T. A. M. Towards high-throughput in situ structural biology using electron cryotomography. *Prog. Biophys. Mol. Biol.* **160**, 97–103 (2021).
12. Danev, R., Yanagisawa, H. & Kikkawa, M. Cryo-Electron Microscopy Methodology: Current Aspects and Future Directions. *Trends Biochem. Sci.* **44**, 837–848 (2019).
13. Turk, M. & Baumeister, W. The promise and the challenges of cryo-electron tomography. *FEBS Letters* **594**, 3243–3261 (2020).
14. Glaeser, R. M. *Specimen Behavior in the Electron Beam*. *Methods in Enzymology* **579**, (Elsevier Inc., 2016).
15. Dubochet, J. & Sartori Blanc, N. The cell in absence of aggregation artifacts. *Micron* **32**, 91–99 (2001).
16. Tivol, W. F., Briegel, A. & Jensen, G. J. An improved cryogen for plunge freezing. *Microsc. Microanal.* **14**, 375–379 (2008).
17. Grimm, R. *et al.* Energy filtered electron tomography of ice-embedded actin and vesicles. *Biophys. J.* **72**, 482–489 (1997).
18. Al-Amoudi, A., Norlen, L. P. O. & Dubochet, J. Cryo-electron microscopy of vitreous sections of native biological cells and tissues. *J. Struct. Biol.* **148**, 131–135 (2004).

19. Marko, M., Hsieh, C., Schalek, R., Frank, J. & Mannella, C. Focused-ion-beam thinning of frozen-hydrated biological specimens for cryo-electron microscopy. *Nat. Methods* **4**, 215–217 (2007).
20. Villa, E., Schaffer, M., Plitzko, J. M. & Baumeister, W. Opening windows into the cell: Focused-ion-beam milling for cryo-electron tomography. *Curr. Opin. Struct. Biol.* **23**, 771–777 (2013).
21. Schaffer, M. *et al.* Optimized cryo-focused ion beam sample preparation aimed at in situ structural studies of membrane proteins. *J. Struct. Biol.* **197**, 73–82 (2017).
22. Klumpe, S. *et al.* A Modular Platform for Automated Cryo-FIB Workflows. *Elife* **10**, 1–29 (2021).
23. Zachs, T. *et al.* Fully automated, sequential focused ion beam milling for cryo-electron tomography. *Elife* **9**, 1–14 (2020).
24. Chang, Y. W. *et al.* Correlated cryogenic photoactivated localization microscopy and cryo-electron tomography. *Nat. Methods* **11**, 737–739 (2014).
25. Wang, L. *et al.* Solid immersion microscopy images cells under cryogenic conditions with 12 nm resolution. *Commun. Biol.* **2**, 1–11 (2019).
26. van Elsland, D. M. *et al.* Ultrastructural Imaging of Salmonella–Host Interactions Using Super-resolution Correlative Light-Electron Microscopy of Bioorthogonal Pathogens. *ChemBioChem* **19**, 1766–1770 (2018).
27. Brilot, A. F. *et al.* Beam-induced motion of vitrified specimen on holey carbon film. *J. Struct. Biol.* **177**, 630–637 (2012).
28. Tegunov, D., Xue, L., Dienemann, C., Cramer, P. & Mahamid, J. Multi-particle cryo-EM refinement with M visualizes ribosome-antibiotic complex at 3.5 Å in cells. *Nat. Methods* **18**, 186–193 (2021).
29. Kuijper, M. *et al.* FEI's direct electron detector developments: Embarking on a revolution in cryo-TEM. *J. Struct. Biol.* **192**, 179–187 (2015).
30. Kühlbrandt, W. The resolution revolution. *Science (80-.).* **343**, 1443–1444 (2014).
31. Hoenger, A. & Bouchet-Marquis, C. Cellular tomography. *Adv. Protein Chem. Struct. Biol.* **82**, 67–90 (2011).
32. Żak, A. Guide to controlling the electron dose to improve low-dose imaging of sensitive samples. *Micron* **145**, (2021).
33. Crowther, R. A., DeRosier, D. J. & Klug, A. The Reconstruction of a Three-Dimensional Structure from Projections and Its Application to Electron Microscopy. *Proc. R. Soc. London* **317**, 318–340 (1970).
34. Grimm, R., Typke, D., Bärmann, M. & Baumeister, W. Determination of the inelastic mean free path in ice by examination of tilted vesicles and automated most probable loss imaging. *Ultramicroscopy* **63**, 169–179 (1996).
35. Hagen, W. J. H., Wan, W. & Briggs, J. A. G. Implementation of a cryo-electron tomography tilt-scheme optimized for high resolution subtomogram averaging. *J. Struct. Biol.* **197**, 191–198 (2017).
36. Eisenstein, F., Danev, R. & Pilhofer, M. Improved applicability and robustness of fast cryo-electron tomography data acquisition. *J. Struct. Biol.* **208**, 107–114 (2019).
37. Harapin, J. *et al.* Structural analysis of multicellular organisms with cryo-electron tomography. *Nat. Methods* **12**, 634–636 (2015).
38. Danev, R. & Baumeister, W. Expanding the boundaries of cryo-EM with phase plates. *Curr. Opin. Struct. Biol.* **46**, 87–94 (2017).
39. Schwartz, O. *et al.* Laser phase plate for transmission electron microscopy. *Nat.*

Methods **16**, 1016–1020 (2019).
40. Chen, M. *et al.* A complete data processing workflow for cryo-ET and subtomogram averaging. *Nat. Methods* **16**, 1161–1168 (2019).
41. Grant, T., Rohou, A. & Grigorieff, N. cisTEM, user-friendly software for single- particle. *Elife* **7**, (2018).
42. Tegunov, D. & Cramer, P. Real-time cryo-electron microscopy data preprocessing with Warp. *Nat. Methods* **16**, 1146–1152 (2019).
43. Kremer, J. R., Mastronarde, D. N. & McIntosh, J. R. Computer visualization of three-dimensional image data using IMOD. *J. Struct. Biol.* **116**, 71–76 (1996).
44. Hrabe, T. *et al.* PyTom: A python-based toolbox for localization of macromolecules in cryo-electron tomograms and subtomogram analysis. *J. Struct. Biol.* **178**, 177–188 (2012).
45. Amat, F. *et al.* Alignment of cryo-electron tomography datasets. *Methods Enzymol.* **482**, 343–367 (2010).
46. Rademaker, M. Weighted Back-projection Methods. in *Electron Tomography* **Second Edi**, 245–271 (2005).
47. Zanetti, G., Riches, J. D., Fuller, S. D. & Briggs, J. A. G. Contrast transfer function correction applied to cryo-electron tomography and sub-tomogram averaging. *J. Struct. Biol.* **168**, 305–312 (2009).
48. Turoňová, B., Schur, F. K. M., Wan, W. & Briggs, J. A. G. Efficient 3D-CTF correction for cryo-electron tomography using NovaCTF improves subtomogram averaging resolution to 3.4 Å. *J. Struct. Biol.* **199**, 187–195 (2017).
49. Himes, B. A. & Zhang, P. emClarity: software for high-resolution cryo-electron tomography and subtomogram averaging. *Nat. Methods* **15**, 955–961 (2018).
50. Zivanov, J. *et al.* A Bayesian approach to single-particle electron cryo-tomography in RELION-4.0. *bioRxiv* (2022).
51. Bepler, T. *et al.* TOPAZ: A Positive-Unlabeled Convolutional Neural Network CryoEM Particle Picker that can Pick Any Size and Shape Particle. *Microsc. Microanal.* **25**, 986–987 (2019).
52. Punjani, A., Rubinstein, J. L., Fleet, D. J. & Brubaker, M. A. CryoSPARC: Algorithms for rapid unsupervised cryo-EM structure determination. *Nat. Methods* **14**, 290–296 (2017).
53. Pyle, E. & Zanetti, G. Current data processing strategies for cryo-electron tomography and subtomogram averaging. *Biochem. J.* **478**, 1827–1845 (2021).
54. Castaño-Díez, D. The Dynamo package for tomography and subtomogram averaging: Components for MATLAB, GPU computing and EC2 Amazon Web Services. *Acta Crystallogr. Sect. D Struct. Biol.* **73**, 478–487 (2017).
55. Moebel, E. *et al.* Deep learning improves macromolecule identification in 3D cellular cryo-electron tomograms. *Nat. Methods* **18**, 1386–1394 (2021).
56. Tang, G. *et al.* EMAN2: An extensible image processing suite for electron microscopy. *J. Struct. Biol.* **157**, 38–46 (2007).
57. Förster, F. & Hegerl, R. Structure Determination In Situ by Averaging of Tomograms. *Methods Cell Biol.* **2007**, 741–767 (2007).
58. O'Reilly, F. J. *et al.* In-cell architecture of an actively transcribing-translating expressome. *Science* **369**, 554–557 (2020).
59. Dandey, V. P. *et al.* Time-resolved cryo-EM using Spotiton. *Nat. Methods* **17**, 897–900 (2020).

60. Alber, F., Förster, F., Korkin, D., Topf, M. & Sali, A. Integrating diverse data for structure determination of macromolecular assemblies. *Annu. Rev. Biochem.* **77**, 443–477 (2008).
61. Bäuerlein, F. J. B. & Baumeister, W. Towards Visual Proteomics at High Resolution. *J. Mol. Biol.* **433**, (2021).
62. Mosalaganti, S. *et al.* Artificial intelligence reveals nuclear pore complexity. *bioRxiv* (2021). doi:https://doi.org/10.1101/2021.10.26.465776
63. Banerjee, A., Bhakta, S. & Sengupta, J. Integrative approaches in cryogenic electron microscopy: Recent advances in structural biology and future perspectives. *iScience* **24**, 102044 (2021).
64. Klykov, O. *et al.* Label-free visual proteomics: Coupling MS- and EM-based approaches in structural biology. *Mol. Cell* **82**, 285–303 (2022).
65. Liu, F., Rijkers, D. T. S., Post, H. & Heck, A. J. R. Proteome-wide profiling of protein assemblies by cross-linking mass spectrometry. *Nat. Methods* **12**, 1179–1184 (2015).
66. O'Reilly, F. J. *et al.* In-cell architecture of an actively transcribing-translating expressome. *Science (80-.).* **369**, 554–557 (2020).
67. Lerner, E. *et al.* FRET-based dynamic structural biology: Challenges, perspectives and an appeal for open-science practices. *Elife* **10**, 1–69 (2021).
68. Korostelev, A. A. The Structural Dynamics of Translation. *Annu. Rev. Biochem.* (2022).
69. Webster, M. W. & Weixlbaumer, A. Macromolecular assemblies supporting transcription-translation coupling. *Transcription* **12**, 103–125 (2021).
70. Stevenson-Jones, F., Woodgate, J., Castro-Roa, D. & Zenkin, N. Ribosome reactivates transcription by physically pushing RNA polymerase out of transcription arrest. *Proc. Natl. Acad. Sci. U. S. A.* **117**, 8462–8467 (2020).
71. Chen, M. & Frederick, K. RNA polymerase's relationship with the ribosome: Not so physical, most of the time. *J. Mol. Biol.* **432**, 3981–3986 (2017).
72. Kohler, R., Mooney, R. A., Mills, D. J., Landick, R. & Cramer, P. Architecture of a transcribing-translating expressome.pdf. *Science* **356**, 194–197 (2017).
73. Zhu, M., Mori, M., Hwa, T. & Dai, X. Disruption of transcription-translation coordination in Escherichia coli leads to premature transcriptional termination. *Nat Microbiol.* **4**, 2347–2356 (2019).
74. Webster, M. W. *et al.* Structural basis of transcription-translation coupling and collision in bacteria. *Science* **369**, 1355–1359 (2020).
75. Burmann, B. M. *et al.* A NusE : NusG Complex Links Transcription and Translation. *Science (80-.).* **328**, 501–505 (2010).